Experimental performances of a 1 kW HPT by means of plasma diagnostics

IEPC-2017-447

Presented at the 35th International Electric Propulsion Conference
Georgia Institute of Technology – Atlanta, Georgia – USA
October 8–12, 2017

Jaume Navarro-Cavallé*, Mick Wijnen†, Pablo Fajardo‡, Mario Merino§ and Eduardo Ahedo¶
Universidad Carlos III Madrid, Leganés, Madrid, 28911, Spain

and

Mercedes Ruiz‖ and Víctor Gómez**
SENER Ingeniería y Sistemas, Tres Cantos, Madrid, 28760, Spain

An experimental Helicon Plasma Thruster developed by EP2 and SENER has been tested in the 300 - 1000 W radiofrequency power range. Several operational sets have been tried with the goal of determining the HPT performances envelope. This has included: Argon and Xenon mass flow rates about 35-100 sccm and 1-30 sccm respectively, different magnetic topologies and strengths, and different radio-frequency antennae shapes. The propulsive performances of this prototype have been indirectly assessed by means of plasmas diagnostics, concluding that the delivered thrust is about 6.6 mN at 500 W.

Nomenclature

B	= magnetic field
m_α , $\alpha = e, i$	= particle mass for electrons or ions
$\dot{m}$	= mass flow rate
n	= plasma density
P	= power
T_e	= electron temperature
x	= transversal distance to the thruster axis
z	= longitudinal distance downstream, on axis, from the HPT05 exit section
η_u	= propellant utilization efficiency
η	= thrust efficiency
ϕ	= plasma potential
θ	= FP view angle of the HPT05 exit section, $\theta = atan(x/z)$

*PhD, Bioengineering and Aerospace Engineering Department, Plasmas and Electric Propulsion Team (EP2), jaume.navarro@uc3m.es.
†PhD Student, Bioengineering and Aerospace Engineering Department, EP2, mwijnen@pa.uc3m.es.
‡Professor, Bioengineering and Aerospace Engineering Department, EP2, pablo.fajardo@uc3m.es.
§Visiting Professor, Bioengineering and Aerospace Engineering Department, EP2, mario.merino@uc3m.es.
¶Full Professor, Bioengineering and Aerospace Engineering Department, EP2, eduardo.ahedo@uc3m.es.
‖Project Manager, Aerospace Division, Mercedes.ruiz@sener.es.
**System Engineer, Aerospace Division, victor.gomez@sener.es.

I. Introduction

The electric propulsion community has invested some effort into the exploration of the Helicon Plasma Thruster (HPT)[1–3] as a reliable technology for in Space Propulsion. Since the first theoretical analyses, most of them coming from the background knowledge on Helicon Sources,[4,5] the HPT has been presented into the community as an advantageous solution against other mature technologies. The lack of electrodes has been stressed recurrently as the greatest benefit in front of Ion Gridded or Hall Effect Thrusters. Furthermore, it is flexible in the propellant choice and throttleable (variable thrust and specific impulse) by tuning its operational parameters. A long lifetime has been claimed thanks to the magnetic screening of its walls, as well as the acceleration stage, which consists in the use of a Magnetic Nozzle (MN) to guide and accelerate supersonically the plasma jet, even deflecting it.[6]

However, most of the performances are still pending of being proved experimentally. On this side, the work of several research institutions may be highlighted, but all of them share either poor performances or results, that even promising, are surrounded by an atmosphere of doubts and uncertainties in their consistency. One of the most fructiferous group, which has been energetically promoting this technology is the Boswell and Charles' team (in the beginnings of the HPT[1,7]), and their co-workers, like Takahashi[8,9] (in the recent times). They have reached thrust efficiencies about 7%[9] in the kW range. In US, most of the Electric Propulsion Laboratories have paid interest into this technology. To cite some of them, the mini Helicon Plasma Experiment at MIT[2] reported a thrust efficiency about 20%, operating in the kW range and higher magnetic fields (> 1000 G) in comparison to others. The Magnetic Nozzle experiment in the EPPDyL (Princeton University) has reported interesting data concerning the plasma structure on the expansion region.[10] Finally, in the old continent, the European Commission financed the HPH.Com project in the 7^{th} Framework Program.[11] That consortium proposed a Helicon Thruster in the low power range, below 100 W, and they reported efficiencies above 10 %.[12]

The work presented here has its foundational basis in an ESA financed project "Helicon Plasma Thruster for Space Missions".[13] After that project the joint-venture EP2 and SENER Ingeniería y Sistemas decided to design,[14] built and test a HPT prototype in the 1 kW range. The design was made according to the EP2 theoretical background on the modelling of the plasma fluid-dynamics within the source,[15] on the plasma plume expansion[16] (Magnetic Nozzle) and also considering a simple 1D model for the radiofrequency wave propagation throughout the magnetized plasma column.[17] The HPT05 was successfully ignited and tested[18] for first time in ESTEC-ESA.[19] Later, its performances have been improved by means of experimentation in the EP2 Space Propulsion Laboratory in Madrid. In this paper, some of the parametric analyses that have been done in the winter-spring 2017 test campaign are reported in order to show the current status of this prototype.

In section II the prototype is presented, underlining the different tested configurations. A brief description of the vacuum facilities and plasma diagnostics are described in Seciton III. The main experimental results are summarized and discussed in Section IV and Section V is for conclusions.

II. HPT05 Platform

The HPT05 breadboard consists of a classical HPT configuration (see Figure 1), composed of: a cylindrical chamber where the plasma is produced; a magnetic circuit to generate the magnetic field, which allows guiding the plasma, coupling radiofrequency (RF) power more efficiently, confining the plasma (keep it away from walls) and expanding it on the MN; a RF system to emit the RF wave; and an injector system to feed the thruster with some neutral gas.

The cylindrical discharge chamber is made of quartz, 3 cm inner diameter and variable length thanks to the use of a moveable injector. The mentioned injector slides manually along the quartz tube and is made of Macor®. This was initially conceived to, apart from injecting the neutral gas, housing an annular Neodymium Permanent Magnet (PM) with the goal of magnetically screening any possible plasma flow moving backwards, thus reducing the plasma wall losses. However, in the work discussed here, all the tests have been performed with an injector version without the PM.

A set of three copper solenoids wrap the quartz tube in order to generate the magnetic field. Two of them (S1 and S2) are devoted to control the field within the tube and the last coil (S3), larger in diameter, controls the field strength of the MN. These coils are hold by means of four aluminum rods which are screwed to an aluminum back plate. The quartz tube is clamped as well to the back plate. A true hole in this plate

allows feeding the injector with the use of an alumina tube.

The RF antenna is placed (in all the results presented in this work) between the S1 and S2 coils. Two different kinds of antennas have been tested, a double loop and a half-turn helical antenna. To feed the antenna with RF power at 13.56 MHz in the 300-900 W power range, a commercial RF generator power unit has been used (RFGPU). The RFGPU consists of a power amplifier, which delivers up to 2 kW (with output impedance $Z_{out} = 50\ \Omega$), and a matching network (π - type configuration), which allows to optimize the power transmission to the load, i.e. the antenna. The amplifier and the matching box are placed outside the vacuum chamber. A combination of a feedthrough (FT) and a coaxial feeder are used to connect the matching output strap with the antenna. For upcoming campaigns, the setup will be upgraded in order to increase the robustness of the system and improve sensing capacity.

The parametric range explored in the aforementioned test campaign has been quite wide. Table 1 summarizes the main parameters that have been tuned and their ranges.

Parameter	**Range**
B_{S1}	0 - 600 G (both directions)
B_{S2}	0 - 600 G (both directions)
B_{S3}	0 - 600 G
$\dot{m}$ **(Ar)**	35 - 100 sccm
$\dot{m}$ **(Xe)**	2 - 30 sccm
L**(chamber length)**	15 - 28 cm
P_{RF}	300 - 900 W

Table 1. Summary of the explored parametric range. B is the magnetic field strength defined at the centre of the coil.

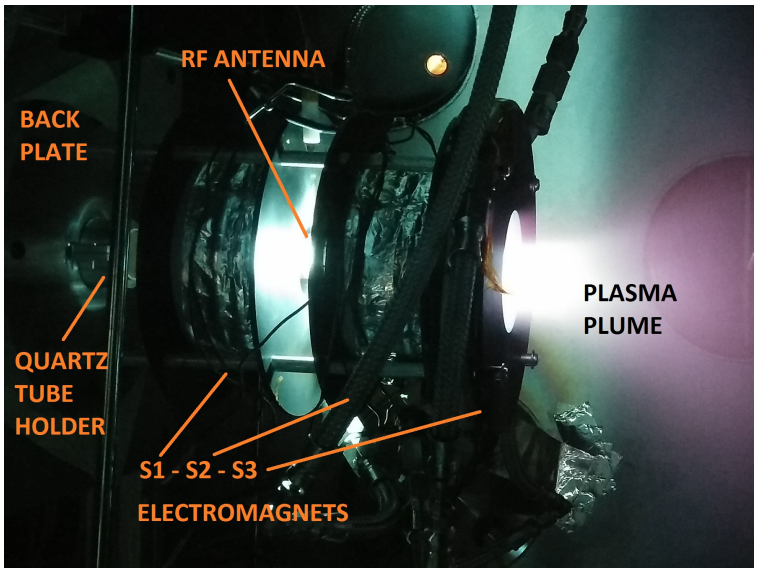

Figure 1. Picture of the HPT05 breadboard operating with Xenon within the vacuum chamber at the EP2 Space Propulsion Laboratory. The injector front face is aligned to the front side of the S1 coil.

III. Experimental facilities

This section describes the novel facilities in the UC3M (Madrid) in which the HPT05 has been tested. The second subsection inquires into the description of the different diagnostics used in this work.

A. Vacuum system

The vacuum chamber in EP2 facilities consists of a non-magnetic stainless-steel 304 vessel of 1.5 m inner diameter and 3.5 m long, as pictured in Figure 2. Three different vacuum technologies are combined to reach an ultimate pressure about 10^{-7} mbar (dry conditions) and $2.5 \cdot 10^{-5}$ mbar (at 20 sccm of Xe/Ar): for the rough vacuum a dry mechanical pump (free-oil technology) Leyvac LV80 with pumping speed about 80 m^3/h decrease the background pressure down to $5 \cdot 10^{-1}$ mbar. Two turbomelecuar pumps, MAGW2.200iP (with magnetically levitated bearings) and pumping speeds up to 2000 l/s each allow reaching pressures in the 10^{-6} mbar range. Finally a set of three cryopanels, Leyvac 140 T-V, allows keeping the pressure in the low 10^{-5} mbar range while operating at moderate mass flow rates, 20 sccm of Xe/Ar. These cyropanels are optimized for Ar (reaching cold temperatures about 17 K) and can be switched to larger panels, optimized for Xe (reaching cold temperatures about 30 K). The total vacuum capacity of the whole system is about 37000 l/s Xe. A Bronkhorst mass flow controller allows to feed the different experiments with neutral gas in the 0-100 sccm range.

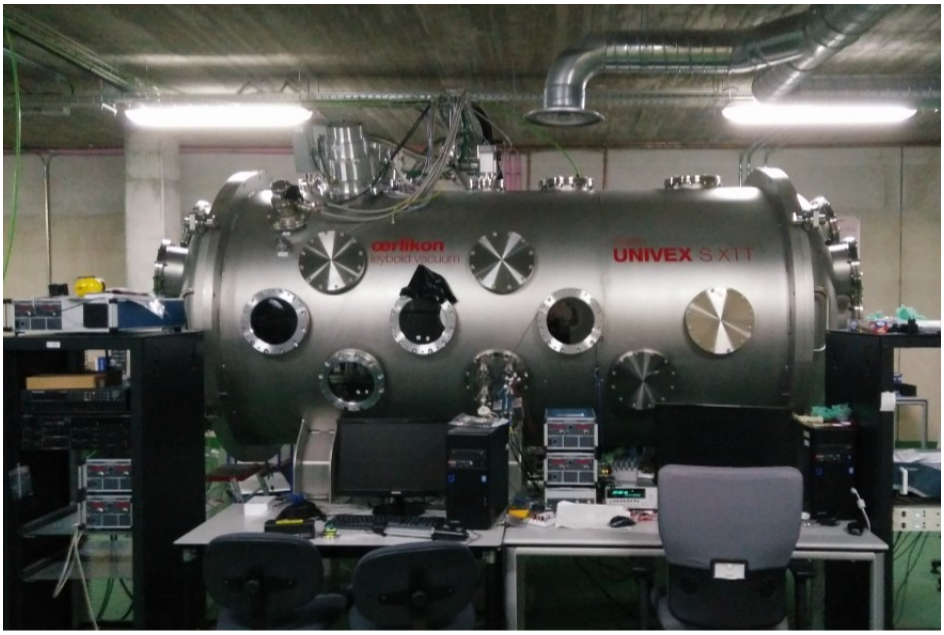

Figure 2. Vacuum chamber in the EP2 Space Propulsion Laboratory, UC3M (Madrid).

B. Plasma Diagnostics

Three different intrusive probes (See Figure 3) have been mounted in an arm system. This system has been developed internally by the EP2 team. The movable arm system allows performing a 3D characterization of the plasma plume ejected by the thruster. This probe holder allows to move the intrusive probes in a Cartesian reference frame, whose origin coincides with the centre of the exhaust section of the tested thruster, in the current case, the HPT05 (centre of the external side of the electromagnet S3).

A simple Langmuir Probe (LP) has been used to measure, mainly, the plasma density n and electron temperature T_e at several positions. The LP tip measures 0.127 mm in diameter and 2 mm length, and it is made of tungsten. In this test campaign the LP has been swept axially and transversely to obtain the axial/radial trends of the aforementioned magnitudes. A radiofrequency compensated Langmuir Probe (RFCLP) has been used as well, although most of the results presented here are only for the simple LP. This is because preliminary tests with the RFCLP have yielded inconsistent results according to the existent theory of LPs and RFCLPs. Allen-Boyd-Reynolds model (ABR),[20] the Bernstein-Rabinowitz-Laframboise model (BRL)[21] and the planar or Bohm model (B), have been used to post-process the I-V characteristic curves acquired with the LP using a high resolution electrometer Keithley 22805-60-3. The plasma potential has been measured directly few times by means of an emissive probe (EP), which has been built in-house and hold in the same arm system.

Finally, a Faraday probe (FP) has also been built and installed on the arm system in order to measure the ion current profile and assess the beam divergence. The FP collector has a radius of 5 mm and it is made of stainless steel. The guard ring, also made of stainless steel, has an inner radius of 5.5 mm and an outer radius of 10 mm. The gap width is therefore 0.5 mm. Considering this geometry, the conservative case (particles can be collected through the gap, and thus it gives the smallest value of current) consists in considering an effective radius of 5.5 mm, resulting a collector area of 95.03 mm^2. However, in the current set-up, because of the use of a "Cartesian arm system", made the estimation of the beam divergence and ion current more difficult. First, because of the transverse movement of the probe (perpendicular to the axis of the thruster), this is not facing the thruster exit, a correction must be applied to the measured current. Second, the range swept by the probe is limited by the chamber width, so it is not possible to scan properly the current at the external wings of the plasma jet. This would require cover a full semi-circle (180 deg) centred at the thruster exit section. For this reason, the EP2 is currently developing a radial-azimuthal arm in order to overcome these limitations. The combination of both systems will offer high flexibility and accuracy on the determination of the plasma structure.

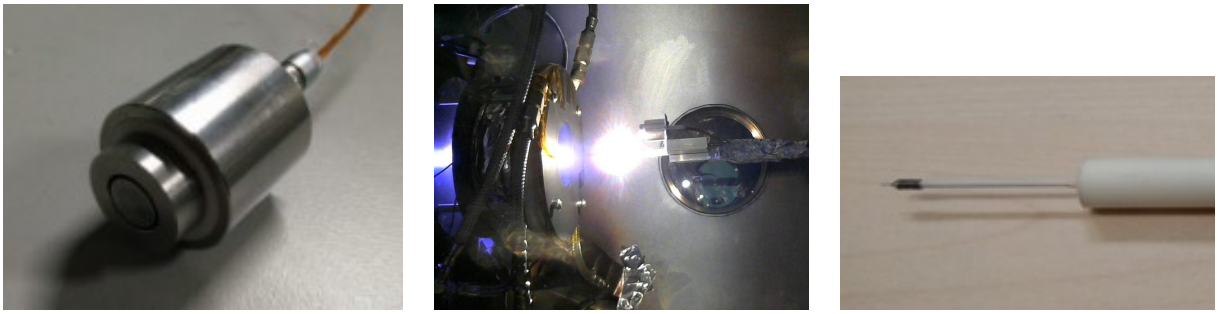

Figure 3. Intrusive diagnostics used during the campaign. From left to right: FP, EP installed on the arm system and RFCLP.

IV. Results

This section summarizes some of the results compiled during the test campaign. The following list enumerates all the issues that will be explored or discussed:

- The propellant utilization efficiency η_u dependence with the Fwd RF power, P_{RF} and mass flow rate $\dot{m}$.
- The plasma density n and electron temperature T_e measured close to the HPT05 exit section ($z = 2$ cm) as $\dot{m}$ is increased.
- The ion current density j transverse profiles for different powers and antenna shapes.
- The role of the magnetic nozzle or S3 field on the beam collimation.
- The visual inspection of the Helicon "blue" mode.
- Theoretical comparison of the on-axis properties.

Figure 4 (left) shows the propellant utilization efficiency with transmitted RF power $\eta_u(P_{RF})$. Here, transmitted means, Forward - Backward RF power, but it is not necessarily the power coupled to the plasma. This is typically lower because of transmission losses throughout the RFGPU components, thermal and radiation losses. This result is for $\dot{m}_{Ar} = 50$ sccm and a magnetic topology determined by $B = -5.3, 12, 16$ Amp (of DC current applied to S1, S2 and S3 coils respectively, hereafter, nominal topology). This figure monotonically rises with no bounds, although the slope of the curve diminishes with P_{RF}, it seems that the HPT05 would allow larger powers, indicating that its response, concerning η_u would probably improve for powers beyond the 1 kW. η_u is depicted as well against different $\dot{m}$ (Argon) for fixed transmitted power $P_{RF} = 800$ W, and nominal B. This plot shows that a threshold for $\dot{m}$ exists and separates the low

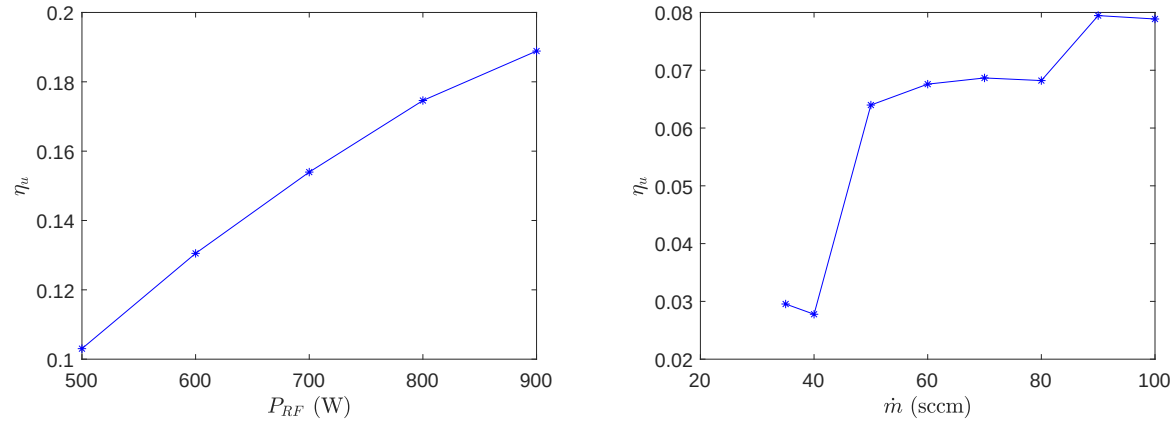

Figure 4. Left: Utilization efficiency $\eta_u(P_{RF})$ against the increase of the delivered RF power to the load, and $\dot{m}_{Ar} = 50$ sccm. Right: Utilization efficiency $\eta_u(\dot{m})$ against the increase of the Ar mass flow rate, at 800 W. For both cases B is set by applying -5.3, 12, 16 Amp on S1/S2/S3 respectively, hereafter nominal configuration, and the double loop antenna is used.

ionization from the high ionization regimes. In the last regime the measured utilization doubles the one at the low ionization regime.

Plasma density n and electron temperature T_e are shown in Figure 5. These variables are measured at $z = 2$ cm from the HPT05 exit section, for different $\dot{m}$ values, and for constant $P_{RF} = 800$ W and nominal B. Plasma density increases an order of magnitude, from below 10^{17} up to close to 10^{18} m^{-3}, within the 40-60 sccm range. At larger mass flow rates, the plasma density increases weaker with $\dot{m}$. $T_e = 4$ eV is almost constant with the increase of $\dot{m}$ except below 60 sccm. The higher T_e for smaller mass flow rates could be induced by the fact that the fitting laws of the I-V characteristic curves according the different tested LP theories might fail or present a larger error, when the plasma density is smaller (Debye sheath expands).

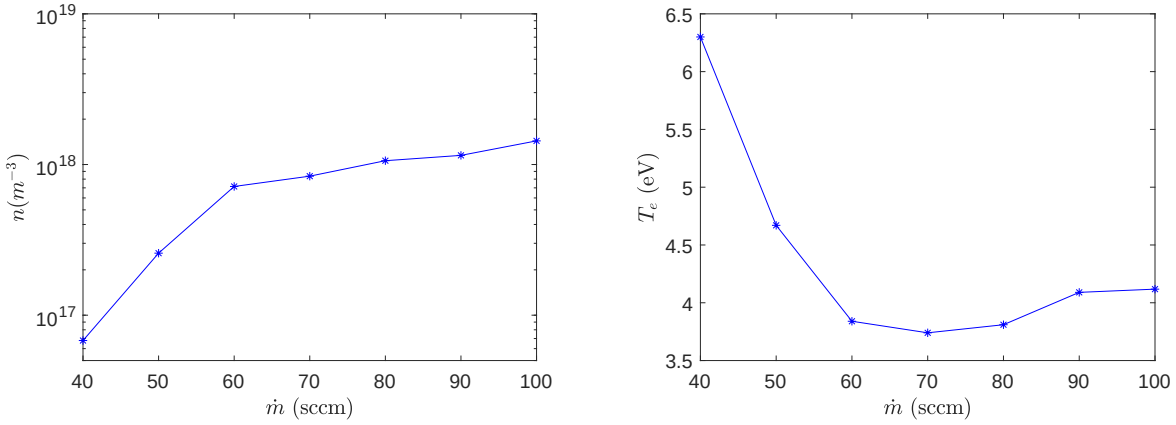

Figure 5. Plasma density $n(\dot{m})$ (left) and electron temperature $T_e(\dot{m})$ measured at $z = 2$ cm (downstream from the HPT05 exit section) as the Ar mass flow rate increases. All other parameters are: $P_{RF} = 800$ W, B nominal, and using double loop antenna.

Ion current density profiles $j_z(x)$ have been obtained by sweeping the FP along the transverse direction, x, biased at $V_{sat} = -30$ V, ion saturation regime. Because the probe is moving along x, it is necessary to correct the collected current. This correction depends on the third power of the $cos(\theta)$. In Figure 6 (left), $j_r(\theta) = j_z(x)/cos^3(\theta)$ is depicted for increasing power. All profiles are normalized against the maximum measured current, $j_{r,max}$, and $z = 20$ cm. For all the cases, $\dot{m} = 50$ sccm and B nominal. It is noticeable the fact that the normalized profiles do not depend on power. This could mean that no power is deposited

onto the plasma in the MN area, instead, all the power is coupled within the discharge chamber. Also note that these profiles are double peaked, which is the common shape for RF inductive plasmas. The effect of the antenna shape on the plasma-wave coupling is underlined in Figure 6 (right). It is observed that the ion current profile is single peak when the half turn helical antenna is used. This means that the wave penetrate to the plasma column more efficiently, in comparison to the double loop antenna. Although the RF power is similar in the cases which are compared, 500 W vs 650 W for the half turn vs the double loop, the B topology is different in each case because it is not possible to set the same nominal field with the use of the helical antenna (plasma discharge jumps down to a low density "capacitive" mode). Both antennas are tested with $\dot{m} = 50$ sccm of Argon.

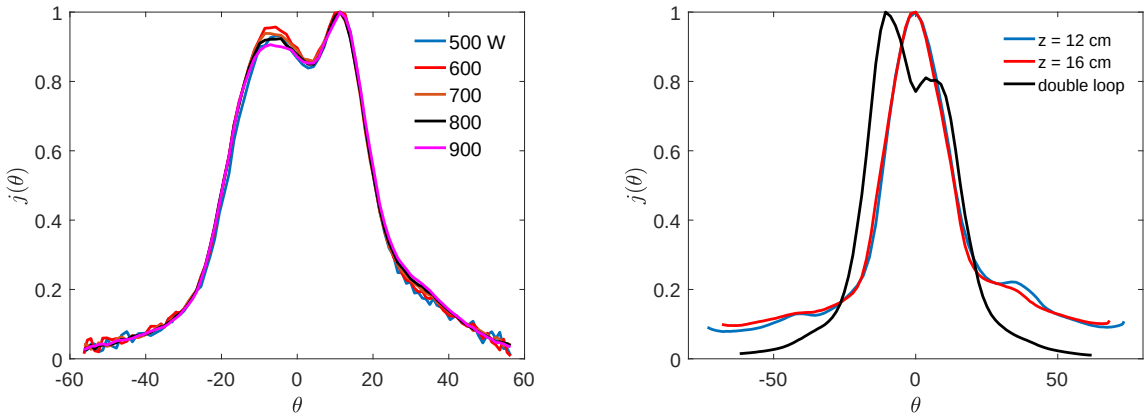

Figure 6. Left: Normalized ion current density profile $j(\theta)(P_{RF})$ measured at $z = 20$ cm, $\dot{m}_{Ar} = 50$ sccm, and B in the nominal configuration. Each profile is normalized against its maximum j_{max}. The current j is corrected because the FP is swept on a perpendicular plane to the HPT05 axis. Then, j is depicted against the angle $\theta = atan(x/z)$, with x the transversal distance measured from the thruster axis, and z the longitudinal distance from the HPT05 exit section. Right: effect of the antenna on the ion current profile. Single peak profiles corresponds to the use of the helical antenna $P_{RF} = 500$ W, $B = 0, -12, -16$ Amp. Double peak profile is for the double loop antenna at $P_{RF} = 650$ W and B nominal. For both antennae $\dot{m}_{Ar} = 50$ sccm.

The effect of the magnetic nozzle (S3 coil) on the beam collimation is illustrated in Figure 7. Beam divergence clearly increases when the magnetic nozzle is turned off, and the other way around, plasma beam focuses on the thruster axis when the MN coil is turned on. These effects are justified by the ion current density profile, but they can be seen by visual inspection as well.

To better visualize the plume divergence a 2D plot was made inspired by similar plot from Little.[22] The plot of Figure 7-(top-right) shows the magnetic flux tubes (30-60-90%) in the $z - r$ plane normalized with magnetic nozzle throat radius. Then the radial ion density profile where measured at several downstream positions. The boundaries of the 30-60-90% flux tubes are calculated and mark in the same plot. It can be seen that 60% of the ion flux lies within the 30% magnetic fluxtubes showing that the ions are detached from the streamlines. The 90% ion flux tubes coincide with the 90% magnetic flux tubes which is not the case for the results of Ref. 22. This is probably an artifact of measuring in a Cartesian coordinate system $(z - r)$ which overestimates the current density at the wings. Measurements obtained with a cylindrical $(\theta - r)$ system should confirm this. Lastly it has to be noted that Little's results are for a 310 G field on-axis at the thruster exit plane as opposed to 560 G for the HPT05.

Finally, most of the researchers claim that the efficient mode, when dealing with Helicon sources, is the so called "blue mode" or Helicon mode. In Figure 8 a snapshot of the HPT05 from downstream is presented. Power was 800 W and $\dot{m} = 50$ sccm. This mode is not obtained for the nominal magnetic field. To proof this mode, the spectra in the visible range is also attached. The spectra shows a large emission in the 350-550 nm range (blue light), that is comparable to the red emission. The blue emission corresponds to the excitation of ArII (singly ionized Argon atoms).

A. Theoretical comparison against DIMAGNO

The axial structure of the plasma density, plasma potential and ion current density, have been compared against the theoretical results of DiMagNo model.[16] This model is a stationary two-fluid model (for electrons

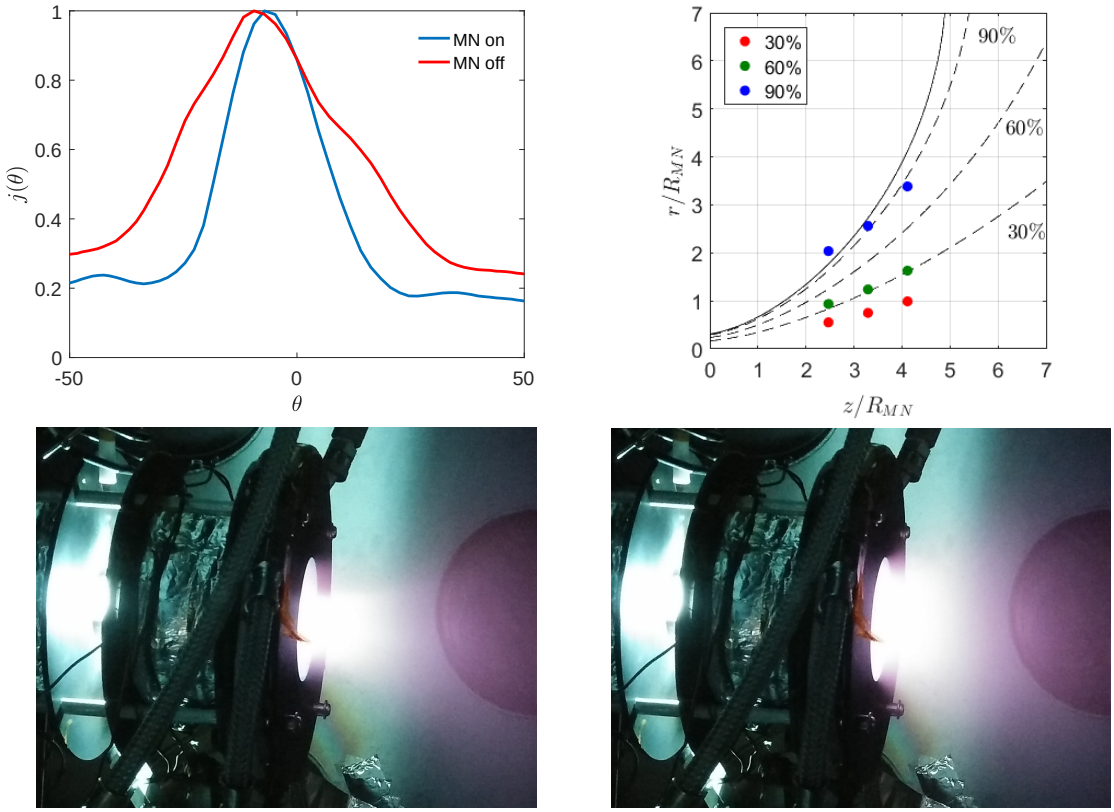

Figure 7. Top-left: Normalized ion current density profile $j(\theta)$ measured at $z = 20$ cm, $\dot{m}_{Ar} = 50$ sccm, and $B = 0, 12, 16/0$ Amp. Each profile is normalized against its maximum j_{max}. Top-right: Bottom: snapshots of the plasma plume. These have been obtained with Xenon at $\dot{m} = 30$ sccm, $P_{RF} = 800$ W and B nominal with MN coil turned on (left) or off (right).

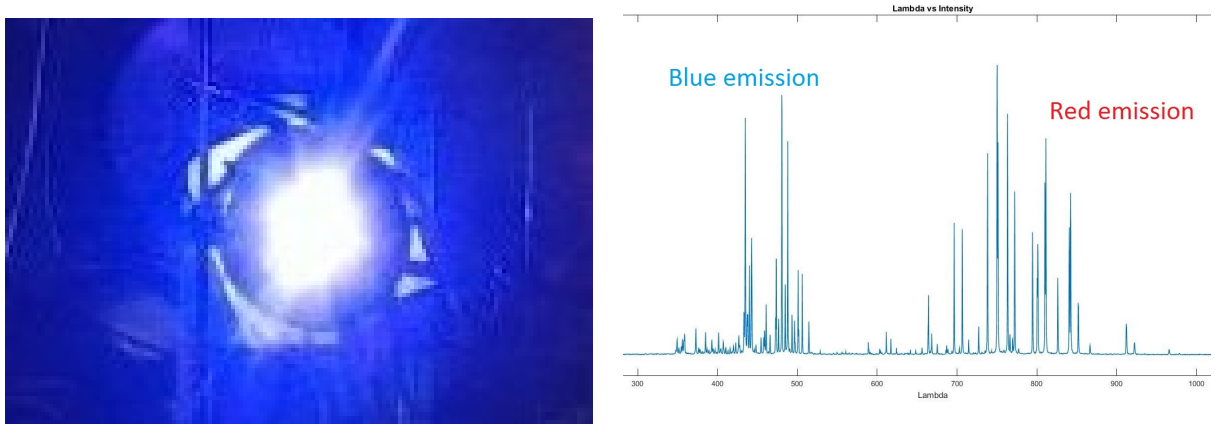

Figure 8. Left: Blue mode with $\dot{m}_{Ar} = 50$ sccm reached at $P_{RF} = 800$ W. Right: optical spectrak (counts, a.u.) for this HPT05 shot that shows a large excitation of ArII (ionized Argon).

and ions) of a fully ionized and quasineutral plasma, that solves its expansion throughout a MN using the method of characteristics. It takes as input the normalized radial profiles of the plasma density, potential, electron temperature and ion Mach number at the MN throat or at a certain section on the supersonic side. This initial front is then propagated downstream; intermediate points can be found by interpolation. Measured radial profiles of the plasma parameters at 4 cm downstream from the HPT05 exit have been used as input for DiMagNo and propagated downstream.

For the Mach number the on-axis value has taken from axial measurements to be about $M = 2$ and the direction was assumed to be parallel to the magnetic field lines; a reasonable assumption so close to the exhaust or MN throat as in the current case. For the electrons thermodynamics, an adiabatic coefficient $\gamma \simeq 1.1$ has been shown as the one that fits better with experimental results.

In Figure 9 simulated plasma properties are compared against the corresponding experimental results. Density measurements taken with the Langmuir probe deviates from the theoretical results. This deviation increases far downstream and this measured density is likely overestimated. To explain this disagreement, we believe that due to the supersonic nature of the analyzed flow, and the fact that the Langmuir probe is aligned with it, this behavior could be induced by charge-exchange collisions. This mechanism may generate low speed ions that would increase the total current collected by the Langmuir probe. Nevertheless, this population is small in comparison to the fast ions, thus not perturbing to much Faraday probe measurements, since this probe is facing this supersonic flow. To check this hypothesis, density is estimated as,

$$n^* = j_{iz}/u_{iz}e, \tag{1}$$

in which j_{iz} is the axial ion current density on-axis measured by the Faraday probe, e is the electron-ion charge and u_{iz} is the ion velocity. This velocity is estimated by assuming that the ion energy is preserved throughout the expansion and this ion flow is sonic at the magnetic throat. This hypothesis combined with the direct measurements of the plasma potential ϕ (emissive probe) allows determining u_{iz} as well as the Mach number,

$$M_{iz} = u_{iz}/c_s = \sqrt{1 + e(\phi_0 - \phi)/kT_e}, \tag{2}$$

being $c_s = \sqrt{T_e/m_i}$ the ion sound speed. ϕ_0 is the potential at the initial section. Using this second approach, the axial density profile agrees much better with the DiMagNo results. Direct measurements of the current density j and plasma potential ϕ are depicted in Figure 9 (right).

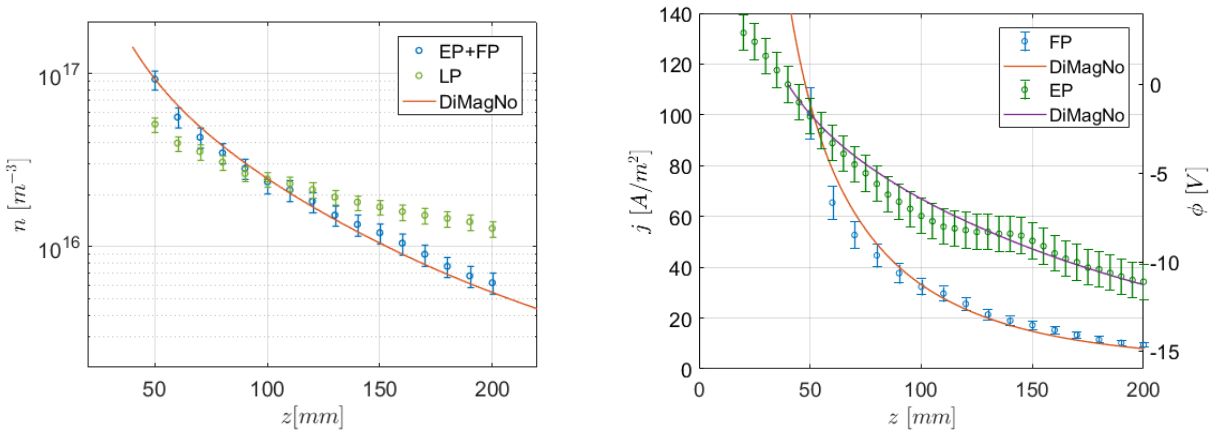

Figure 9. Axial density profiles. Ion current density and plasma potential axial profiles.

B. HPT05 Performances discussion

Hereafter, we discuss and summarize some of the propulsive figures that have been assessed based on the experimental data. Regarding the propellant utilization, the highest value has been obtained at 500 W, with 1.5 mg/s of Xenon, $\eta_u = 23$ %; and 18 % for 1.5 mg/s of Argon at 900 W. Extrapolating the Xenon results with power, we suggest $\eta_u \sim 50$ % at 900 W and 1.5 mg/s.

Concerning the beam divergence, the increase of beam collimation due to the applied field in the MN coil has been proved. However, for the current HPT05 prototype, the half divergence angle is estimated to be larger than 50 deg, in spite of increasing the MN field.

By adding to the previous results the two-dimensional plume characterization, which has consisted in measuring the spatial structure of the plasma plume properties for different parametric sets of the HPT05 prototype, the overall HPT05 thrust and thrust efficiency are assessed. These 2D maps are not presented in this manuscript, and only few axial trends have been shown above. Evaluating the plasma momentum at $z = 20$ cm, we estimate a total thrust around 6.6 mN, for 500 W and 1.5 mg/s of Argon. Considering that the effective power delivered by the antenna could be in the 100-500 W range because of power losses in the RFGPU transmission lines, the thrust efficiency would be in the 2.9-14% range. The specific impulse for these values is roughly 448 s.

V. Conclusions

A first experimental campaign of the HPT05 prototype in the EP2 new facilities has been carried out with acceptable success. The HPT05 propulsive performances in the explored range have been determined to be quite poor, and it is still necessary to clarify uncertainties in the plasma response. Getting a full image of the plasma structure within the source and in the plasma plume has been underlined as a must necessity in order to determine the guidelines for the optimization of this prototype. The EP2 team is working on the definition of the HPT05 upgrading. On the other side, most of the problems regarding the weak plasma-wave coupling points out the RFGPU (feeding lines and connections) as the responsible of these poor performances. For this reason SENER is currently working on the RFGPU upgrade.

Acknowledgments

The authors acknowledge the financial support of *Airbus Defence and Space* to the testing activities carried out in UC3M facilities (Contract CW241842) and to R. Albertoni for the careful reading of this manuscript. This work has been also supported by the National research and development programme of Spain, Project ESP2016-75887.

References

[1]Charles, C. and Boswell, R., "Current-free double-layer formation in a high-density helicon discharge," *Applied Physics Letters*, Vol. 82, No. 9, 2003, pp. 1356–1358.

[2]Batishchev, O., "Minihelicon Plasma Thruster," *IEEE Transaction on Plasma Science*, Vol. 37, 2009, pp. 1563–1571.

[3]et al, D. P., "Thruster Development Set-up for the Helicon Plasma Hydrazine Combined Micro Research Project (HPH.com)," *32nd International Electric Propulsion Conference, Wiesbaden, Germany*, Vol. IEPC-2011-241, 2011.

[4]Boswell, R., "Very efficient plasma generation by whistler waves near the lower hybrid frequency," *Plasma Physics and Controlled Fusion*, Vol. 26, 1984, pp. 1147–1162.

[5]Chen, F., "Plasma ionization by helicon waves," *Plasma Physics and Controlled Fusion*, Vol. 33, 1991, pp. 339.

[6]Merino, M. and Ahedo, E., "Contactless steering of a plasma jet with a 3D magnetic nozzle," *Plasma Sources Sci. Technol*, Vol. 26, No. 095001, 2017, pp. 095001.

[7]Charles, C., Boswell, R., and Lieberman, M., "Xenon ion beam characterization in a helicon double layer thruster," *Applied Physics Letters*, Vol. 89, 2006, pp. 261503.

[8]Takahashi, K., Lafleur, T., Charles, C., Alexander, P., and Boswell, R., "Electron Diamagnetic Effect on Axial Force in an Expanding Plasma: Experiments and Theory," *Physical Review Letters*, Vol. 107, No. 23, 2011, pp. 235001.

[9]Takahashi, K., Charles, C., Boswell, R., and Ando, A., "Performance improvement of a permanent magnet helicon plasma thruster," *Journal of Physics D: Applied Physics*, Vol. 46, No. 35, 2013, pp. 352001.

[10]Little, J. M. and Choueiri, E. Y., "Critical Condition for Plasma Confinement in the Source of a Magnetic Nozzle Flow," *IEEE Transactions on Plasma Science*, Vol. 43, No. 1, 2015, pp. 277–286.

[11]Pavarin, D., Ferri, F., Manente, M., Curreli, D., Guclu, Y., Melazzi, D., Rondini, D., Suman, S., Carlsson, J., Bramanti, C., Ahedo, E., Lancellotti, V., Katsonis, K., and Markelov, G., "Design of 50W Helicon Plasma Thruster," *31th International Electric Propulsion Conference, Ann Arbor, Michigan, USA*, edited by F. Electric Rocket Propulsion Society, IEPC 2009-205, 2009.

[12]"HPH.COM Final Report," Tech. rep., European Commission, 7^{th} Framework Programme, 2012.

[13]Navarro Cavalle, J., Gómez, V., Ahedo, E., Merino, M., Sanchez, G., and Ruiz, M., "HPT for Space Missions," Tech. rep., 2015.

[14]Merino, M., Navarro, J., Casado, S., Ahedo, E., Gómez, V., Ruiz, M., Bosch, E., and del Amo, J., "Design and

development of a 1 kW-class helicon antenna thruster," *34th International Electric Propulsion Conference, IEPC-2015-297 (Electric Rocket Propulsion Society, Fairview Park, OH, 2015)*, 2015.

[15]Ahedo, E. and Navarro-Cavalle, J., "Helicon thruster plasma modeling: Two-dimensional fluid-dynamics and propulsive performances," *Physics of Plasmas*, Vol. 20, 2013, pp. 043512.

[16]Ahedo, E. and Merino, M., "Two-dimensional supersonic plasma acceleration in a magnetic nozzle," *Physics of Plasmas*, Vol. 17, 2010, pp. 073501.

[17]Tian, B., Ahedo, E., and Navarro-Cavalle, J., "Investigation of Plasma-wave Interaction in Helicon Antenna Thrusters," *The 50th AIAA/ASME/SAE/ASEE Joint Propulsion Conference& Exhibit, AIAA Paper*, 2014-3475, 2014.

[18]Merino, M., Navarro, J., Ahedo, E., Gómez, V., Sánchez, V., Ruiz, M., Dannenmayer, K., Bosch, E., and González, J., "Maiden tests of the HPT05 helicon plasma thruster prototype," *Space Propulsion Conference 2016*, No. 3125014, 2016.

[19]del Amo, J. G., Saccoccia, G., and Frigot, P., "ESA propulsion lab at ESTEC," *31st International Electric Propulsion Conference*, 2009.

[20]Allen, J., Boyd, R., and Reynolds, P., "The collection of positive ions by a probe immersed in a plasma," *Proceedings of the Physical Society. Section B*, Vol. 70, No. 3, 1957, pp. 297.

[21]Laframboise, J. G., "Theory of spherical and cylindrical Langmuir probes in a collisionless, Maxwellian plasma at rest," Tech. rep., TORONTO UNIV DOWNSVIEW (ONTARIO) INST FOR AEROSPACE STUDIES, 1966.

[22]Little, J. M. and Choueiri, E., "Influence of the Applied Magnetic Field Strength on Flow Collimation in Magnetic Nozzles," *50th AIAA/ASME/SAE/ASEE Joint Propulsion Conference*, 2014, p. 3912.